



# Collagen-like Motifs of SasG: A Novel Fold for Protein Mechanical Strength

Alexander J. E. Bruce, Emanuele Paci<sup>†</sup> and David J. Brockwell<sup>\*</sup>

Astbury Centre for Structural and Molecular Biology and School of Molecular and Cellular Biology, Faculty of Biological Sciences, University of Leeds, LS2 9JT, UK

Correspondence to David J. Brockwell: [D.J.Brockwell@leeds.ac.uk](mailto:D.J.Brockwell@leeds.ac.uk) (D.J. Brockwell)  
<https://doi.org/10.1016/j.jmb.2023.167980>

Edited by C. Kalodimos

## Abstract

The *Staphylococcus aureus* surface protein G (SasG) is associated with host colonisation and biofilm formation. As colonisation occurs at the liquid-substrate interface bacteria are subject to a myriad of external forces and, presumably as a consequence, SasG displays extreme mechanical strength. This mechanical phenotype arises from the B-domain; a repetitive region composed of alternating E and G5 subdomains. These subdomains have an unusual structure comprising collagen-like regions capped by triple-stranded  $\beta$ -sheets. To identify the determinants of SasG mechanical strength, we characterised the mechanical phenotype and thermodynamic stability of 18 single substitution variants of a pseudo-wildtype protein. Visualising the mechanically-induced transition state at a residue-level by  $\phi$ -value analysis reveals that the main force-bearing regions are the N- and C-terminal ‘Mechanical Clamps’ and their side-chain interactions. This is tailored by contacts at the pseudo-hydrophobic core interface. We also describe a novel mechanical motif – the collagen-like region and show that glycine to alanine substitutions, analogous to those found in *Osteogenesis Imperfecta* (brittle bone disease), result in a significantly reduced mechanical strength.

© 2023 The Author(s). Published by Elsevier Ltd. This is an open access article under the CC BY license (<http://creativecommons.org/licenses/by/4.0/>).

## Introduction

Bacteria typically populate liquid-substrate interfaces, rather than bulk liquid, by the formation of biofilms – a bacterial community encapsulated in an extracellular polysaccharide substance.<sup>1–2</sup> The attachment and growth of bacteria to the substrate during biofilm formation is usually mediated by cell-surface structures such as cell-wall anchored (CWA) proteins through binding of their A (adhesin) domains to cognate host ligands.<sup>3–5</sup> These interactions are typically strong and long lasting, such as the interaction between the *Staphylococcal* surface protein SpsD and fibrinogen, which boasts a bond strength of 1.8 nN measured by Atomic Force Microscopy (AFM) at a retraction velocity of 1000 nms<sup>-1</sup>.<sup>5</sup> As these adhesion:ligand

interactions rupture at forces similar to covalent bonds,<sup>6</sup> the remaining structure may either be expected to extend under tensile force (to reduce the load on the non-covalent adhesin-ligand bond to extend lifetime) or to exhibit high mechanical strength. For example, type 1 pili are helical rods composed of 1000 globular subunits utilised by *E. coli* to attach to the host epithelium.<sup>7</sup> Under external force, pili extend reversibly by unwinding of the helical quaternary structure. In contrast, the E and G5 subdomains of the *Staphylococcus epidermidis* accumulation-associated protein (Aap) (a ‘periscope’ protein<sup>8</sup>) sequentially unfold at extreme forces of ~312 and ~475 pN, respectively, prior to adhesion:ligand bond dissociation (~3 nN at 1000 nms<sup>-1</sup>).<sup>9</sup> In a similar fashion, the E and G5 subdomains from the analogous CWA ‘periscope’ protein,

SasG, also exhibit remarkable mechanostability, unfolding at  $\sim 230$  and  $\sim 380$  pN at  $1500 \text{ nm s}^{-1}$  using the AFM.<sup>10</sup>

SasG is a multi-domain protein thought to promote host colonisation and biofilm formation<sup>11–14</sup> and comprises a host-ligand binding A domain<sup>11</sup> and a B domain of 3–10 tandemly arrayed B-repeats<sup>15</sup> (Figure 1(A)). Each B-repeat is formed from one copy each of structurally related E and G5 subdomains.<sup>16</sup> These subdomains have an unusual flat elongated structure, comprising three interlaced strands forming a collagen-like region, which is capped by a triple stranded  $\beta$ -sheet with a mixed parallel/anti-parallel arrangement<sup>16</sup> (Figure 1(B)). The interfaces between the E and G5 subdomains are compact and the presence of hydrophobic side chains forms a pseudo-hydrophobic core.<sup>16</sup> The collagen-like motif (CLM) comprises a mixed parallel/antiparallel PPII-like chain arrangement leading to a staggered distorted triple helix resembling the structure of collagen but involving a single polypeptide chain only (Figure 1(C)).<sup>17</sup> The triple helical structure of collagen (a right-handed triple helix comprising left-handed helical polypeptides) is known to perform a mechanical function in vertebrates, but its complex quaternary structure has hindered previous investigations of collagen mechanical properties at the single-molecule level.<sup>18</sup> Consequently, characterisation of the mechanical effects of amino-acid substitutions associated with Osteogenesis Imperfecta (OI) a disease of the connective tissues characterised by extremely fragile bones has not been investigated at the single-molecule level.

Which of the unusual structural features of SasG endow the observed extreme mechanical strength of this protein? Single-molecule force spectroscopy (SMFS) is a powerful tool for

delineating the effect of force at the molecular level. SMFS permits the measurement of force response to changes in the end-to-end length of a protein. In general, all  $\alpha$ -helical proteins or local helical regions are the most mechanically labile (unfolding at a low force or in the noise of the instrument), followed by  $\alpha/\beta$  structures, with all  $\beta$ -proteins exhibiting the highest mechanostability.<sup>19–20</sup> The most mechanically stable proteins share a common shear topology whereupon two directly hydrogen-bonded  $\beta$ -strands are extended in opposite directions parallel to the  $\beta$ -strand long-axis. This requires the simultaneous rupture of hydrogen bonds between the  $\beta$ -strands creating a ‘mechanical clamp’ motif.<sup>21–23</sup> Several of the most mechanically robust proteins characterised to date are derived from bacterial extracellular repetitive Immunoglobulin (Ig)-like fold domains including the scaffoldin c7A domain<sup>24</sup> and the SdrG B1 domain.<sup>25</sup> The mechanostability of the latter is enhanced by the coordination of  $\text{Ca}^{2+}$  ions across the hydrogen bonded ‘mechanical clamp’, as also observed for the extender domains of *MpAFP* and *MhLap* adhesion proteins.<sup>26</sup> Instead of mechanical stability enhancement by non-covalent bridging across  $\beta$ -strands, the formation of post-translational isopeptide bonds across the terminal strands of Spy0128<sup>27</sup> and the Cna B domain<sup>28</sup> renders them mechanically inextensible. In addition to topology, hydrophobic contacts across the shearing mechanical interface have also been shown to tailor mechanical stability in protein L<sup>29</sup> and protein GB1.<sup>30</sup>

The B-domains of SasG lack many of the canonical features of ‘mechanically strong’ proteins: directly hydrogen bonded  $\beta$ -strands are not sheared, there is no typical hydrophobic core, known metal ion coordination or intramolecular

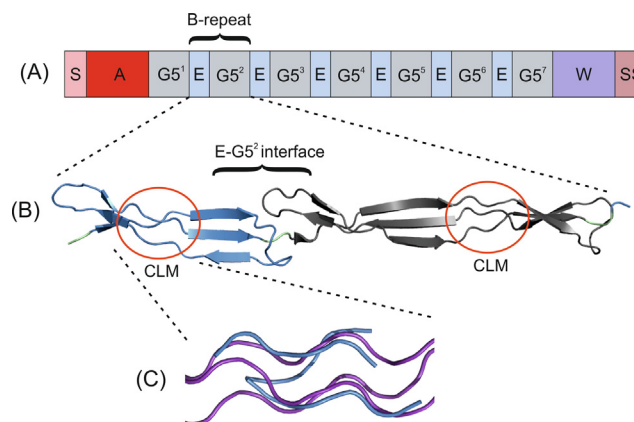


**Figure 1.** Domain arrangement of full length SasG and structural details of a B-repeat domain. (A) Schematic of full-length SasG. S: Signal sequence, A: A domain, W: Wall-spanning region and SS: Sorting signal. A single B-repeat is highlighted. (B) E-G5<sup>2</sup> crystal structure (PDB: 3TIP) displaying the structural similarity between the subdomains E and G5<sup>2</sup>. E and G5<sup>2</sup> shown in blue and grey, respectively. The collagen-like motifs (CLM) of the E and G5<sup>2</sup> subdomains are highlighted with a red circle. (C) Collagen-like region (from PDB: 3TIP, coloured blue) aligned with collagen (PDB: 1BKV, coloured purple) to display the collagen-like homology and the staggering of 1/3 strands.

covalent crosslinks, suggesting the presence of novel mechanical motif(s). Previous molecular dynamic (MD) forced unfolding simulations suggested, however, that the mechanical strength originates from the previously described mechanical clamps motifs and the associated side-chain packing interactions between the  $\beta$ -strands.<sup>10</sup>

Here, we created a pentameric pseudo-wildtype polyprotein of the second B-repeat of SasG (pWT (E-G5<sup>2</sup>)<sub>5</sub>) that enabled the rapid generation of 18 variants containing single residue substitutions introduced throughout the secondary structural motifs of SasG. AFM force spectroscopy combined with measurement of thermodynamic stability allowed the identification of residues key to the extreme mechanostability of SasG and visualisation of the mechanical unfolding transition state (TS) by  $\phi$ -value analysis. SasG mechanical stability is multi-faceted as substitutions in the E-G5<sup>2</sup> interface and previously identified 'mechanical clamp' regions significantly destabilised the G5<sup>2</sup> and/or E subdomain. Additionally, we identify a novel mechanical motif – the collagen-like region and show that the same glycine to alanine substitutions that are found in OI also result in a drastically reduced mechanical strength of SasG, directly linking genotypic changes to the mechanical phenotype of a collagen-like structure.

## Results

### Construction, over-expression and biophysical characterisation of a pentameric E-G5<sup>2</sup> homo-polyprotein

The determinants of protein mechanical strength are usually investigated by comparing changes in unfolding force upon single amino acid substitutions introduced into different sequence or structural motifs.<sup>27,29–31</sup> For SasG, however, the high DNA sequence similarity across the tandem B-repeats within the wild-type SasG sequence from *S. aureus* 8325–4 (~97%) and that of a synonymous sequence for expression in *E. coli* (~80%) precluded this approach.

Previous studies on the wild-type (WT) SasG sequence (G5<sup>1</sup>-G5<sup>7</sup>, Figure 2(A)) showed that, in contrast to chemical denaturant induced cooperative (un)folding of B-repeats, the mechanical unfolding of each G5 subdomain was uncoupled from the corresponding E subdomain.<sup>10</sup> Despite this, each E subdomain requires a C-terminal G5 subdomain to form a stable, folded structure.<sup>10,32</sup> Accordingly, a recombinant pentameric homo-polyprotein was designed as a pseudo-WT protein, termed pWT (E-G5<sup>2</sup>)<sub>5</sub> (Figure 2(B)). Each repeat within the pentamer comprised the second G5 subdomain of SasG and its N-terminal E domain (E-G5<sup>2</sup>, residues Glu500 to Tyr625 using the numbering system of 3TIP<sup>10</sup>) with each B-repeat (Figure 2(C)) separated by unstruc-

tured linkers<sup>33</sup> (Figure 2(B)). Following gene construction and protein over-expression (Methods), pWT (E-G5<sup>2</sup>)<sub>5</sub> was purified using a standard three-step purification procedure (Methods), yielding 2–10 mg of soluble protein per L of culture medium. Full details of the DNA and protein sequences can be found in the Supporting Information. Biophysical analysis indicated pWT (E-G5<sup>2</sup>)<sub>5</sub> was folded with a secondary structure content similar to SasG (Figure S1). Furthermore, when pWT (E-G5<sup>2</sup>)<sub>5</sub> was subjected to equilibrium denaturation analysis, a single transition was observed (Figure S2) with identical parameters to monomeric E-G5<sup>2</sup> (Table S1).<sup>10,32</sup> This demonstrates that in equilibrium chemical denaturation experiments, the E and G5<sup>2</sup> subdomains within each repeat unfold cooperatively, but each E-G5<sup>2</sup> repeat unfolds independently (acts as monomeric units).

### pWT (E-G5<sup>2</sup>)<sub>5</sub> as a model to investigate SasG mechanical strength

To validate pWT (E-G5<sup>2</sup>)<sub>5</sub> as a suitable substitute for SasG in SMFS studies, force-extension profiles (obtained as shown schematically in Figure S3) were measured for both pWT (E-G5<sup>2</sup>)<sub>5</sub> (Figure 2(D) and native SasG (Figure S4) at a retraction velocity of 1500 nm s<sup>-1</sup> using the AFM in PBS, pH 7.4 in triplicate for both constructs (data summarised in Tables S2–S5). Gene construction, protein over-expression and purification is outlined in Supporting Information, Tables S2–S5. The 'sawtoothed' force-extension profile for pWT (E-G5<sup>2</sup>)<sub>5</sub> displayed five smaller peaks then five larger peaks, followed by a detachment peak (Figure 2(D)). The numbers of each subdomain unfolding event reflect the composition of pWT (E-G5<sup>2</sup>)<sub>5</sub> (Figure 2(B)). Each force-extension profile was described well by the worm-like chain (WLC) model<sup>34–35</sup> allowing the change in contour length ( $\Delta L_C$ , corresponding to the total length of amino acids 'released' upon unfolding) for each unfolding event to be determined. This gave average values of  $147.7 \pm 2.9$  and  $214.7 \pm 1.2$  Å for the E and G5<sup>2</sup> subdomains, respectively, in close agreement to those measured for the E ( $150.5 \pm 3.7$  Å) and G5 ( $218.1 \pm 4.3$  Å) subdomains of native SasG. Comparison of the unfolding forces for G5 ( $F_{U,G5}$ ) and E ( $F_{U,E}$ ) domains reveal a small but significant increase in  $F_{U,G5}$  for pWT (E-G5<sup>2</sup>)<sub>5</sub> relative to SasG (431.5 and 408.4 pN, respectively), yet a small, but significant decrease in  $F_{U,E}$  (238.5 and 258.4 pN for pWT (E-G5<sup>2</sup>)<sub>5</sub> and SasG, respectively).

$F_U$  is strongly affected by the polyprotein in which the protein domains under study reside.<sup>36</sup> Firstly, the fewer G5 subdomains in pWT (E-G5<sup>2</sup>)<sub>5</sub> relative to SasG (five versus seven) reduces the number of thermally assisted unfolding attempts per unit of time resulting in a greater observed unfolding force. Secondly, the reduced number of domains (either folded or unfolded) reduces the compliance of the

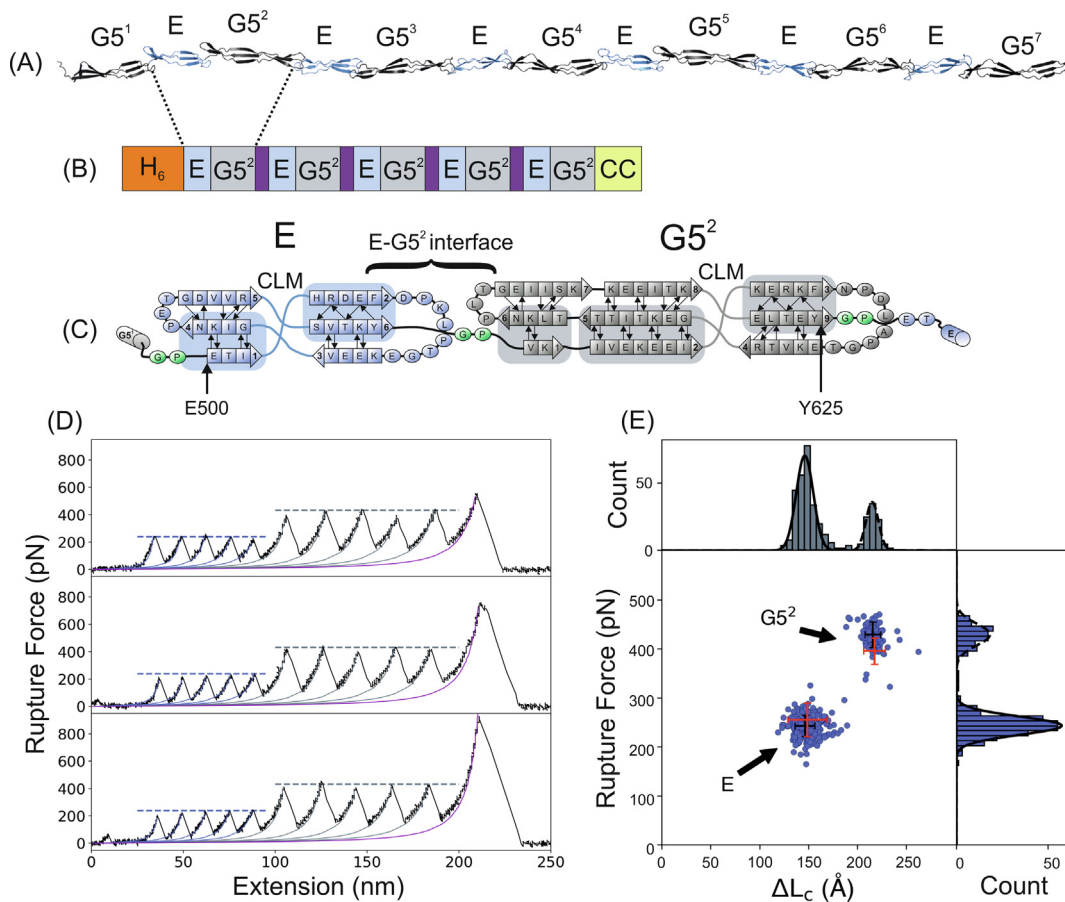


**Figure 2.** The mechanical properties of pWT (E-G5<sup>2</sup>)<sub>5</sub>. (A) Modelled structure of WT SasG G5<sup>1</sup>-G5<sup>7</sup> (taken from reference<sup>10</sup>) with the E-G5<sup>2</sup> B-repeat used in this study highlighted. (B) Schematic of pWT (E-G5<sup>2</sup>)<sub>5</sub> with the E and G5<sup>2</sup> subdomains highlighted in blue and grey, respectively. Linkers (purple), His tag (H<sub>6</sub>, orange) and the C-terminal double cysteine (CC, yellow) are displayed as blocks. (C) Topology diagram of E-G5<sup>2</sup> highlighting boundary residues for E and G5<sup>2</sup>, with GP linker residues highlighted in green. Putative 'mechanical clamp' regions are displayed as blue and grey boxes. (D) Three example pWT (E-G5<sup>2</sup>)<sub>5</sub> 'sawtooth' force-extension profiles (black) displaying five unfolding events of both E and G5<sup>2</sup> subdomains at a retraction velocity of 1500 nm s<sup>-1</sup>. Solid lines: WLC model fitted to E and G5<sup>2</sup> subdomains (blue and grey, respectively), and the detachment peak (purple). The average unfolding forces for pWT (E-G5<sup>2</sup>)<sub>5</sub> E and G5<sup>2</sup> at a retraction velocity of 1500 nm s<sup>-1</sup> are shown as blue and grey dashed lines, respectively. (E) Scatterplot with associated histograms reveals a bimodal distribution in both rupture force and  $\Delta L_C$  values. E and G5<sup>2</sup> Gaussian fits in black solid and dashed lines, respectively. Black scatterplot crosshairs are the mode and the FWHM (full width at half maximum) from the corresponding histogram Gaussian model fits, and red scatterplot crosshairs are the mode and the FWHM from the corresponding histogram Gaussian model fits (not shown here) from an example replicate of SasG at the equivalent retraction velocity.

polyprotein increasing the effective loading rate, resulting in an increase in  $F_U$ . These effects would also be expected to increase  $F_{U,E}$  for pWT (E-G5<sup>2</sup>)<sub>5</sub> but to a lesser extent (five versus six E subdomains in pWT (E-G5<sup>2</sup>)<sub>5</sub> and SasG, respectively). To investigate the origins of the decrease in  $F_{U,E}$  for pWT (E-G5<sup>2</sup>)<sub>5</sub> relative to SasG, forced unfolding was further performed at retraction velocities of 200, 800, 3000 and 5000 nm s<sup>-1</sup> (Tables S2-S5). The difference in  $F_{U,E}$  values for pWT (E-G5<sup>2</sup>)<sub>5</sub> and SasG was found to increase upon increasing retraction velocity (Figure S5). The decrease in the speed dependence of  $F_{U,E}$  for pWT (E-G5<sup>2</sup>)<sub>5</sub>

suggests a change in the underlying energy landscape (a small increase in the  $x_U$  value or the distance from the native state well to the mechanical TS barrier). This is sometimes interpreted as a more mechanically 'malleable' protein.<sup>19</sup> This effect has been observed previously for constructs of different domain number, for example a recombinant I27 octamer (I27<sub>8</sub>) displayed a larger  $x_U$  value than its recombinant pentameric (I27<sub>5</sub>) counterpart.<sup>37</sup> Alternatively, the origin of this difference may be due to the loss of G5-E interfaces between each mechanical E-G5 unit. As the mechanical strength of SasG will be delineated by quantifying the effect of amino-

acid substitutions in the same pWT (E-G5<sup>2</sup>)<sub>5</sub> background, these effects are obviated.

### Selection and the structural and mechanical analysis of variants

Guided by previously obtained thermodynamic and kinetic folding data,<sup>32</sup> eighteen E-G5<sup>2</sup> variants were designed and assembled into pentamers using Golden Gate cloning (Methods) and subjected to SMFS to identify the mechanically-

stabilising motifs in SasG (Figure 3(A)). These substitutions were introduced into the E-G5<sup>2</sup> interface; the collagen-like region and the putative ‘mechanical clamps’ (Figure 2(C)). After construction, each variant was expressed and purified as described for pWT (E-G5<sup>2</sup>)<sub>5</sub> and their identity verified by liquid chromatography-mass spectroscopy (LC-MS) (Table S6). The secondary and tertiary structure of each variant was shown to be similar to pWT (E-G5<sup>2</sup>)<sub>5</sub> using far-UV circular dichroism and fluorescence emission spectroscopy, respectively (Fig-

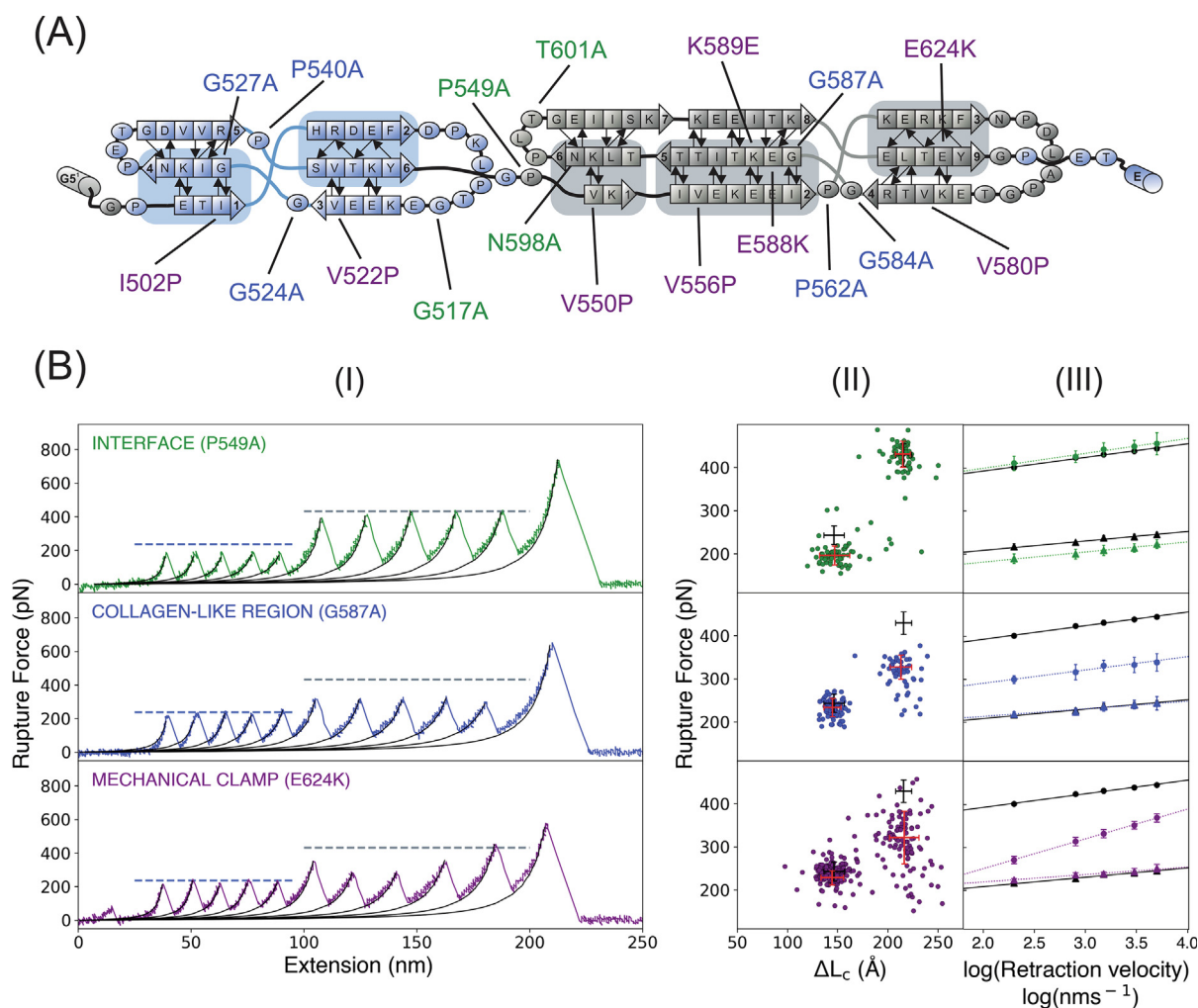


**Figure 3.** Variant location and example SMFS data. (A) Topology diagram of E-G5<sup>2</sup> showing location of each substitution labelled according to the type of mechanical motif: green (interface residue), blue (collagen-like region) or purple (‘mechanical clamp’). The putative ‘mechanical clamp’ regions are shaded in blue or grey. (B) Example data for interface (P549A), collagen-like motif (G587A) and ‘Mechanical Clamp’ (E624K) variants. (I) Force extension profiles where the dashed blue and grey lines correspond to the average unfolding force of the E and G5<sup>2</sup> subdomains of pWT (E-G5<sup>2</sup>)<sub>5</sub>, respectively. The fits to a WLC model are displayed as solid black lines. (II) F<sub>U</sub>-ΔL<sub>c</sub> scatterplots at a retraction velocity of 1500 nms<sup>-1</sup>, where red crosshairs are the mode and FWHM from Gaussian fits to corresponding frequency histograms (not shown). Crosshairs from one repeat at the same retraction velocity are shown for pWT (E-G5<sup>2</sup>)<sub>5</sub> for reference (black). (III) Speed dependence of measured unfolding force, where the points (triangles (lower forces) and circles (higher forces) represent E and G5<sup>2</sup>, respectively) and errors are the mean and standard deviation of triplicate datasets, respectively. The linear fit (broken lines in their respective colour) is weighted with the inverse of the standard deviation error of the triplicate data sets, and pWT (E-G5<sup>2</sup>)<sub>2</sub> data is displayed in black for reference. Full data sets are found in [Supplementary Information](#).

ures S6-S11), with the exception of three of the variants within the 'mechanical clamp' motif of the E (V522P and I502P) and G5<sup>2</sup> subdomain (V550P) (discussed below). Finally, the effects of each substitution on thermodynamic stability was measured by equilibrium denaturation in urea and the resulting fluorescence emission intensity data fit to a two-state model to extract the stability ( $\Delta G_{UN}$ ) and  $m_{UN}$  value (related to the solvent accessible surface area upon unfolding<sup>38</sup> for pWT (E-G5<sup>2</sup>)<sub>5</sub> and variants for which spectroscopy suggested significantly altered/unfolded structures. The  $m_{UN}$  value was fixed at 6 kJ mol<sup>-1</sup> M<sup>-1</sup> (the value extracted for pWT (E-G5<sup>2</sup>)<sub>5</sub>) for all other variants (Figure S12 and Table S1).

Forced unfolding experiments were then carried out in triplicate at five retraction velocities to quantify the speed dependence of the  $F_U$  values for each variant. This is necessary to identify substitutions which induce significant changes to  $x_U$ , characterised by changes in the gradient of a plot of  $F_U$  versus log retraction velocity. For each replicate, at least 20 unfolding events for both E and G5<sup>2</sup> subdomains were accumulated (note the average number of unfolding events for E and G5<sup>2</sup> subdomains was 101 ± 45 and 75 ± 32, respectively, Tables S7-S40). Example force-extension profiles and  $F_U$  versus log retraction velocity plots for a variant from each category are shown in Figure 3(B) and all variants in Figures S13-19 (these figures also show the location of each variant in SasG). All variants, with the exception of V522P (E-G5<sup>2</sup>)<sub>5</sub> and V550P (E-G5<sup>2</sup>)<sub>5</sub> displayed unfolding spectra comprising five unfolding events for both E and G5<sup>2</sup> subdomains and a detachment peak. These two variants typically displayed a featureless force-extension profile for ~90 nm (Figure S17), then five unfolding peaks with  $\Delta L_C$  values identical to that for the G5<sup>2</sup> subdomain (216.9, 215.4 and 214.7 ± 1.8 Å, for V522P, V550P and pWT (E-G5<sup>2</sup>)<sub>5</sub> at 5000 nms<sup>-1</sup>, respectively). These data, together with changes in their CD spectra and a significant reduction in the thermodynamic parameter  $m_{UN}$  to values (4.0 ± 0.1 and 4.1 ± 0.3 kJ mol<sup>-1</sup> M<sup>-1</sup>, Table S1) close to that for G5<sup>2</sup> in isolation (4.2 ± 0.2 kJ mol<sup>-1</sup> M<sup>-1</sup>)<sup>32</sup> suggests that substitution for proline at positions 522 and 550 results in unfolding of the E subdomain. These two variants were not studied further. For all other variants,  $\Delta L_C$  values (Table S41) were within error to that for pWT (E-G5<sup>2</sup>)<sub>5</sub>, indicating the pathway to unfolding is coarsely the same to pWT (E-G5<sup>2</sup>)<sub>5</sub> as a similar amount of structure is being 'released' after unfolding.

### Similar substitutions result in diverse mechanical phenotypes

The aim of this study was to identify the residues and structural motifs that endow SasG mechanical strength. To do this, the average values of  $F_{U,E}$  and  $F_{U,G5}$  and the speed dependences of variants

containing substitutions introduced into each structural motif were calculated. ANCOVA analysis was used to identify variants with a significantly different mechanical phenotype to pWT (E-G5<sup>2</sup>)<sub>5</sub> ( $p < 0.05$ ). For those variants that displayed a significant mechanical difference yet a pWT-like speed dependence (and therefore TS placement, characterised by  $F_U$  versus log retraction velocity plots parallel to those for pWT (E-G5<sup>2</sup>)<sub>5</sub>), a threshold difference in  $F_U$  of at least 12.0 and 21.5 pN for E and G5<sup>2</sup> subdomains (5% error to take into account the intrinsic cantilever calibration error and number of replicates) was used to identify those residues important for mechanical strength.

**E-G5<sup>2</sup> interface variants.** The E-G5 interface is important for both the thermodynamic stability and co-operativity between each subdomain.<sup>10,32</sup> To investigate its role in mechanical unfolding where each subdomain is uncoupled, we designed homo-E-G5<sup>2</sup> pentamers containing single amino-acid substitutions in the E subdomain (G517A), the short GP linker (P549A) and in G5<sup>2</sup> (N598A and T601A) (Figure 3(A)). Despite the large change in thermodynamic stability ( $\Delta\Delta G_{UN} = 13.7 \pm 0.8$  kJ mol<sup>-1</sup>) measured for T601A (E-G5<sup>2</sup>)<sub>5</sub>, its mechanical phenotype was identical to pWT (E-G5<sup>2</sup>)<sub>5</sub> (Figures S12 and S14). Both G517A (E-G5<sup>2</sup>)<sub>5</sub> and P549A (E-G5<sup>2</sup>)<sub>5</sub> displayed a significant decrease in the mechanical strength of the E subdomain across all retraction velocities (e.g.  $\Delta F_U = 22.0 \pm 11.2$  and  $29.0 \pm 13.0$  pN at a retraction velocity of 1500 nms<sup>-1</sup>, respectively) (Figures S13 and S14). P549 is located in the short GP linker connecting E to G5<sup>2</sup> and is part of the pseudo-hydrophobic core interacting with P510 of E and P599 and I605 of G5<sup>2</sup> (Figure S20), also forming a main chain hydrogen bond with G517. Substitutions at these positions may thus affect mechanical strength by changing the packing of the pseudo-hydrophobic core. Finally, a significant increase in the speed dependence of the unfolding force for the E subdomain was observed for N598A (Figure S14). N598 is located in the N-terminal region of the G5<sup>2</sup> subdomain (Figure 3(A)) yet changes were only observed for the E subdomain. This observation, together with the effect of P549A, suggests that despite their mechanical independence, changes to the E-G5<sup>2</sup> interface affects the mechanical strength of the E subdomain, irrespective of its subdomain location with E-G5<sup>2</sup>.

**Collagen-like region variants.** Next, given the known mechanical function of collagen, we sought to identify the role of the collagen-like region in the mechanical strength of SasG. Substitutions of glycine or proline with alanine were introduced into either the E (G524A, G527A and P540A) or G5<sup>2</sup> subdomains (G584A, G587A and P562A) to affect the packing (Gly to Ala) or to disrupt the PPII-like

twists of this region (Pro to Ala). Irrespective of their location, all Gly to Ala variants displayed large decreases in mechanical strength but localised to the subdomain where the substitution was introduced (Figures S15 and S16). For example, a substitution in the E subdomain (G524A) resulted in  $\Delta F_U$  values of  $31.3 \pm 10.1$  and  $3.4 \pm 8.2$  pN at  $1500 \text{ nms}^{-1}$  for E and  $G5^2$  unfolding events, respectively, while G587A ( $G5^2$  subdomain) resulted in  $\Delta F_{U,E}$  and  $\Delta F_{U,G5}$  values of  $1.9 \pm 11.2$  and  $99.7 \pm 14.0$  pN, respectively. In contrast to these results, the consequences on the mechanical behaviour of proline to alanine substitutions within each subdomain (P540A (E subdomain) and P562A ( $G5^2$  subdomain)) were found to be distinct, even though changes in their thermodynamic stability were both small ( $\Delta\Delta G_{UN} = 0.1$  and  $2.3 \text{ kJ mol}^{-1}$ , respectively). More specifically, the force-extension profiles (Figure S15) and speed dependence of  $F_U$  for both E and  $G5^2$  subdomains for P540A ( $(E-G5^2)_5$ ) was similar to pWT ( $(E-G5^2)_5$ ) (Figure S16). By contrast, substituting alanine for proline at residue 562 in  $G5^2$  resulted in a  $\sim 40$  pN decrease in  $F_{U,G5}$  (with no significant change in  $F_{U,E}$ ) at all retraction velocities (Figures S15 and S16). P540 and P562 are located on distinct strands of the structurally similar E and  $G5^2$  subdomains (Figure 3(A)), suggesting differences in force propagation through each strand of the collagen-like region (see  $\phi$ -value analysis below).

**'Mechanical clamp' variants.** To assess the role of the mixed  $\beta$ -sheets in SasG mechanical strength, proline substitution and charge reversal mutants were introduced into each subdomain to disrupt the main-chain hydrogen bonding networks and side-chain charge interactions of the 'mechanical clamps' in the E and  $G5$  subdomains previously identified using MD<sup>10</sup> (Figure 3(A)). The five hydrophobic residue to proline substitutions characterised were I502P and V522P (E subdomain), and V550P, V556P and V580P ( $G5^2$  subdomain). As described above, the E subdomain for V522P and V550P was unfolded at equilibrium (even though residue 550 is in  $G5^2$ ) as assessed by spectroscopic and thermodynamic analysis (Figures S10-S12). Accordingly, only five peaks corresponding to  $G5^2$  was a typical observation in force-extension profiles for these variants (Figure S17). The ability of V550P to prevent E subdomain folding can be rationalised by the observation that the E subdomain will only fold after the interface between E and  $G5^2$  has been formed,<sup>32</sup> suggesting that V550P interferes with interface formation. The mechanical phenotype of V556P (Figures S17 and S19) was found not to be statistically significantly different to pWT ( $(E-G5^2)_5$ ), despite the large change in thermodynamic stability ( $\Delta\Delta G_{UN} = 14.1 \pm 0.8 \text{ kJ mol}^{-1}$ , Table 1).

The remaining two proline substitution variants were found to display different mechanical phenotypes. For I502P (substitution in the E subdomain), a  $\Delta F_{U,E} \sim 50$  pN at all retraction velocities was observed, with the  $G5^2$  subdomain unaffected (Figures S17 and S19). As the spectroscopic evidence (Figure S11) suggests partial unfolding of the E subdomain (with a high probability of this being the 'unlatching' of a  $\beta$ -strand), this large decrease in mechanical strength suggests a role of the 'mechanical clamp' motif in the mechanical strength of the E subdomain. A valine to proline substitution at residue 580 in  $G5^2$  resulted in a change to the speed dependence of  $F_{U,G5}$  while  $F_{U,E}$  was unaffected (Figures S17 and S19). These data suggest that introduction of proline into the  $\beta$ -strands of the mechanical clamp can result in a perturbed unfolding pathway as observed previously.<sup>39</sup> The increase in the gradient of speed dependence of  $F_{U,G5}$  indicates a decrease in  $x_U$  contrasting with the effects of valine to proline mutations in  $\beta$ -sheets of other proteins that display an increase in  $x_U$ .<sup>39</sup>

The mechanical clamp region of  $G5^2$  was also probed by charge-swap substitutions E588K, K589E and E624K. As expected for this type of substitution, all three resulted in large reductions in thermodynamic stability ( $\sim 6$ – $18 \text{ kJ mol}^{-1}$ , Table 1 and Supplementary Table S1) yet the mechanical unfolding behaviour of E588K was indifferently from pWT ( $(E-G5^2)_5$ ) (Figure S18 and S19). K589E resulted in a large decrease ( $\Delta F_{U,G5} \sim 70$  pN) in mechanical strength across all retraction velocities. As biophysical analysis suggests no difference in the native secondary or tertiary structure (Figures S10 and S11), we can speculate that the side chain interactions of K589 are part of the electrostatic packing of the predicted N-terminal 'Mechanical Clamp' of  $G5^2$ .

Similarly for the majority of other variants in this study, while large differences were observed for the subdomain hosting the substitution ( $G5^2$  in this case, see below), no differences in unfolding behaviour relative to pWT ( $(E-G5^2)_5$ ) was observed for the other subdomain (E in this case), evidencing the robustness of our data accumulation and analysis (Table 1). The E624K  $G5^2$  subdomain displayed an intriguing mechanical phenotype. In addition to only the  $G5^2$  subdomain displaying a large decrease in mechanical strength and a substantial change in gradient (Figure 3BIII),  $F_{U,G5}$  values for each unfolding event were observed to vary significantly both within and between approach-retract cycles (Figure S21). As a consequence of this heterogeneity, the width of  $F_{U,G5}$  force-frequency distribution is significantly wider than for pWT ( $(E-G5^2)_5$ ) (Figure S22) (i.e. the average FWHM values are  $\sim 116$  and  $\sim 57$  pN for E624K and pWT ( $(E-G5^2)_5$ ), respectively). Additionally, the average  $\Delta L_C$  distribution was significantly wider for the

Table 1 Thermodynamic and mechanical stability of variants and their mechanical  $\phi$ -values. Mechanical  $\phi$ -values describing the TS of the (E-G5<sup>2</sup>)<sub>5</sub> variants in this study with a pWT-like speed dependence.

Group	Variant	Subdomain Location of mutation	$\Delta\Delta G_{UN}$ (kJ/mol) <sup>a</sup>	$\Delta F_{U,E}$ <sup>b</sup>	$\Delta F_{U,G5}$ <sup>b</sup>	$\phi_E$	$\phi_{G5}$
I	G517A	E	5.6 ± 0.8	<b>22.0 ± 11.2</b>	5.5 ± 17.2	<b>0.5 ± 0.1</b>	0.9 ± 0.2
	P549A	GP Linker	3.8 ± 0.8	29 ± 13.0	-11.8 ± 16.3	0.1 ± 0.0	1.2 ± 0.3
	N598A	G5 <sup>2</sup>	16.7 ± 0.9	22.5 ± 6.1	<b>8.1 ± 11.9</b>	ND	<b>1.0 ± 0.1</b>
	T601A	G5 <sup>2</sup>	13.7 ± 0.8	-6.1 ± 9.2	<b>11.6 ± 14.0</b>	1.1 ± 0.2	<b>0.9 ± 0.1</b>
CLM	G524A	E	6.4 ± 0.8	<b>31.3 ± 10.1</b>	3.4 ± 8.2	<b>0.4 ± 0.1</b>	1.0 ± 0.1
	G527A	E	4.9 ± 0.8	<b>41.6 ± 11.5</b>	-3.5 ± 17.3	<b>0.0 ± 0.0</b>	1.1 ± 0.2
	P540A <sup>c</sup>	E	0.1 ± 0.8	<b>-6.1 ± 10.0</b>	-7.5 ± 8.9	ND	ND
	P562A <sup>d</sup>	G5 <sup>2</sup>	2.3 ± 0.8	-1.9 ± 5.2	<b>34.7 ± 6.4</b>	1.1 ± 0.4	<b>-0.1 ± 0.0</b>
	G584A	G5 <sup>2</sup>	17.7 ± 0.9	-4.1 ± 7.6	<b>42.6 ± 9.7</b>	1.0 ± 0.1	<b>0.8 ± 0.1</b>
	G587A	G5 <sup>2</sup>	20.7 ± 0.9	1.9 ± 9.1	<b>99.7 ± 14.0</b>	1.0 ± 0.1	<b>0.7 ± 0.1</b>
MC	I502P	E	11.2 ± 1.1	<b>50.3 ± 7.0</b>	3.7 ± 7.8	<b>0.5 ± 0.1</b>	1.0 ± 0.1
	V522P <sup>e</sup>	E	15.6 ± 0.9	-	-	ND	ND
	V550P <sup>e</sup>	G5 <sup>2</sup>	17.7 ± 0.9	-	-	ND	<b>1.0<sup>f</sup></b>
	V556P	G5 <sup>2</sup>	14.1 ± 0.8	8 ± 14.6	<b>0.6 ± 9.3</b>	0.9 ± 0.1	<b>1.0 ± 0.1</b>
	V580P	G5 <sup>2</sup>	12.7 ± 0.8	-5.3 ± 11.6	<b>20.8 ± 13.2</b>	1.0 ± 0.2	ND
	E588K	G5 <sup>2</sup>	5.7 ± 0.8	-4.1 ± 10.8	<b>-0.3 ± 8.5</b>	1.1 ± 0.2	<b>1.0 ± 0.2</b>
	K589E	G5 <sup>2</sup>	16.8 ± 0.9	-3.8 ± 6.7	<b>73.8 ± 15.8</b>	1.0 ± 0.1	<b>0.7 ± 0.1</b>
	E624K	G5 <sup>2</sup>	17.7 ± 0.9	-0.8 ± 6.5	<b>99.2 ± 11.4</b>	1.0 ± 0.1	ND

<sup>a</sup>  $\Delta\Delta G_{UN} = \Delta G_{UN,pWT} - \Delta G_{UN,Mut}$  ( $\pm$ propagated error of fit). <sup>b</sup>  $\Delta F_U = F_{U,pWT} - F_{U,Mut}$  at 1500 nms<sup>-1</sup> ( $\pm$ propagated standard deviation). <sup>c</sup>  $\phi$ -value was not calculated due to small change in  $\Delta\Delta G_{UN}$ . <sup>d</sup> P562A (E-G5<sup>2</sup>)<sub>5</sub> has a small  $\Delta\Delta G_{UN}$  value, which can cause artefactual  $\phi$ -values,<sup>44,48</sup> so this should be analysed with caution. <sup>e</sup> V522P and V550P were only unfolded at retraction velocities of 200 and 5000 nms<sup>-1</sup>, so the accurate unfolding force at 1500 nms<sup>-1</sup> is unknown. <sup>f</sup> As V550P (E-G5<sup>2</sup>)<sub>5</sub> displayed mechanical unfolding forces of the G5<sup>2</sup> subdomain indifferent from pWT (E-G5<sup>2</sup>)<sub>5</sub> at unfolding forces of 200 and 5000 nms<sup>-1</sup> (Table S13), we can assume the distance to TS is the same and as there is no change in the activation energy to unfolding (unperturbed mechanical strength), we can estimate the  $\phi$ -value is  $\sim 1$ . Bolded values are those calculated for the subdomain in which the substitution is located. Italicised values are partial  $\phi$ -values and indicate structural perturbation/loss of contacts in the mechanical unfolding TS. As the E subdomain of N598A and G5<sup>2</sup> subdomain of V580P and E624K displayed a change in their speed dependence gradient, the  $\phi$ -value was not calculated. I: interface, CLM: collagen-like motif, MC: 'mechanical clamp', and ND: not done. All errors are propagated.

E624K G5<sup>2</sup> subdomain compared to pWT (E-G5<sup>2</sup>)<sub>5</sub> ( $\sim 28$  vs  $\sim 15$  Å) (Figure S23), indicating there is a larger variety in amount of structure released prior to the detected unfolding peak. These observations offer strong evidence for alternative unfolding pathway(s) for the E624K G5<sup>2</sup>,<sup>40-43</sup> despite a similar CD spectrum to pWT (E-G5<sup>2</sup>)<sub>5</sub> (Figure S10), presumably due to destabilisation of the C-terminal 'mechanical clamp' (Figure 2(C)) by changes to the charge network. Interestingly, Gruszka and colleagues observed that the Y625W variant of monomeric E-G5<sup>2</sup> folded via a distinct pathway.<sup>32</sup> Together with our SMFS data, this suggests that interactions in this region are pivotal for both folding and forced unfolding of G5<sup>2</sup>.

### Revealing the mechanical TS structure through $\phi$ -value analysis

The data above shows that introduction of amino-acid substitutions at specific locations within all three regions can have profound effects on the mechanical strength of SasG (Figure 4(A)). Additionally, while some of these exert their effect by destabilising the ground state, as exemplified by G584A ( $\Delta F_{U,G5} = \sim 40$  pN,  $\Delta\Delta G_{UN} = 17.7 \pm 0.9$  kJ mol<sup>-1</sup>), others show similar changes in unfolding force, with small changes in  $\Delta G_{UN}$  (e.g. P562A  $\Delta F_{U,G5} = \sim 35$  pN,  $\Delta\Delta G_{UN} = 2.3 \pm$

0.8 kJ mol<sup>-1</sup>). The latter variant exerts its effect on the TS. By comparing the relative effects of mutation on the ground state and TS, mechanical  $\phi$ -value analysis<sup>40</sup> has allowed visualisation of the mechanically-induced TS of proteins including I27,<sup>44</sup> TNfn3,<sup>45</sup> Protein L<sup>29</sup> and Protein GB1.<sup>30</sup> As mechanical unfolding experiments probe the local kinetic stability between two defined points, such transition states are usually distinct from those probed by chemical denaturation experiments.<sup>44</sup> In mechanical  $\phi$ -value analysis,  $\Delta F_U$  values can be used to assess the change in kinetic stability as the change in unfolding rate constant is proportional to the change in  $F_U$  relative to the WT if both show similar speed dependences of their unfolding force (i.e. similar placement of the transition state along the unfolding pathway) as other parameters that control loading rate are identical.<sup>40,46</sup> This is discussed further in the Supplemental methods. The  $\phi$ -value is defined as the ratio of change in the height of the TS barrier of mechanical protein unfolding ( $\Delta\Delta_{TS-N}^{WT-MUT}$ ), which is obtained from the measured unfolding force (Methods) to the change in free energy difference between the folded and unfolded state of the protein ( $\Delta\Delta G_{UN}$ ) (measured by equilibrium denaturation) as defined:

$$\phi = 1 - \left( \frac{\Delta\Delta_{TS-N}^{WT-MUT}}{\Delta\Delta G_{UN}} \right)$$

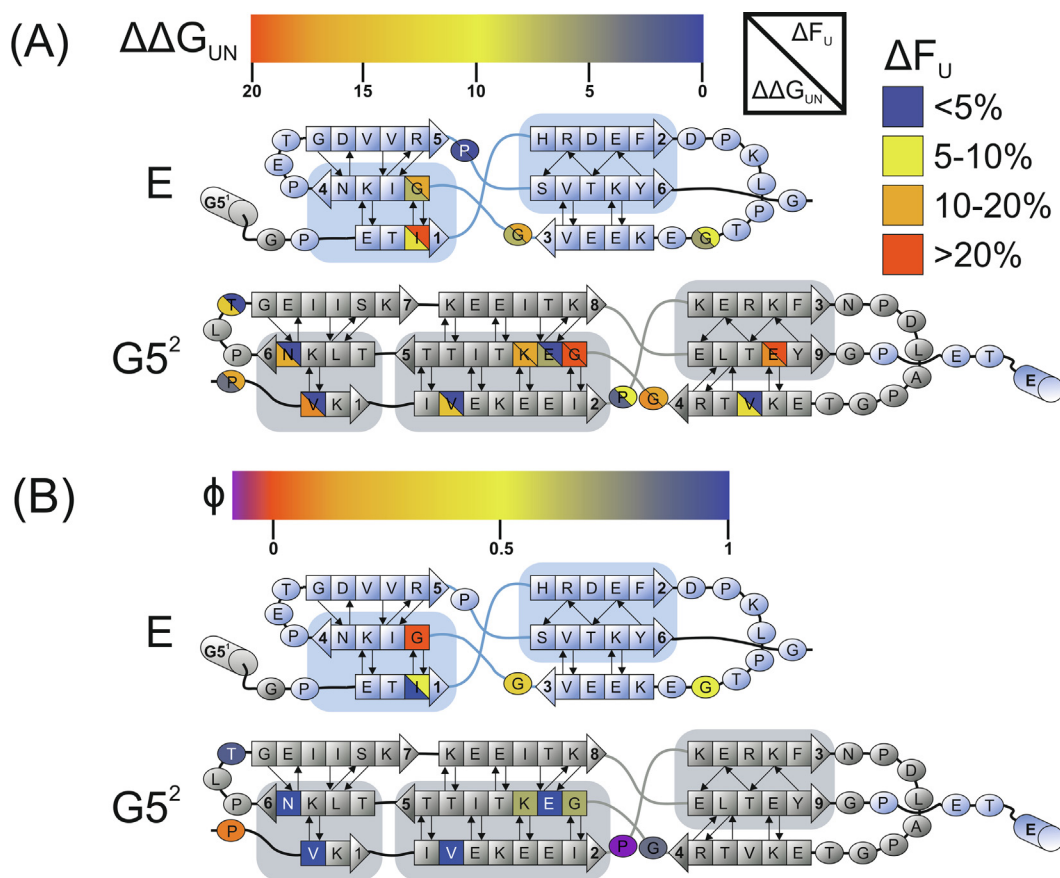


**Figure 4.** Comparison of  $\Delta F_U$ , mechanical  $\phi$ -value and  $\Delta\Delta G_{UN}$  of E-G5<sup>2</sup> variants. Topology diagrams displaying the (A) decrease in mechanical strength relative to pWT (E-G5<sup>2</sup>)<sub>5</sub> at a retraction velocity of 1500 nms<sup>-1</sup> vs  $\Delta\Delta G_{UN}$  values and the (B) mechanical  $\phi$ -values for the variants of E-G5<sup>2</sup>. Comparison of these schematics shows that the majority of the substitutions are exerting their effects on the ground state, whereas P562A is acting on the TS. \*I502P is displayed as both 0.5 and ~1 as spectroscopic evidence suggests partial unfolding of the structure in the native state (Figures S10B and S11B), which implies a value of 0.5 may be an artefact and could actually be closer to ~1 at this residue.<sup>47</sup> V550P is assumed to have a < 5% decrease in the mechanical strength of G5<sup>2</sup> as the unfolding force at 200 and 5000 nms<sup>-1</sup> remain unchanged.

These mechanical  $\phi$ -values describe the structural preservation of the residue's local environment at the mechanical TS upon the application of force, with a value of 0 and 1 indicating the interactions to be fully unformed or fully formed, respectively, with partial  $\phi$ -values indicating partial structuring/contacts. To maintain native-like structure,  $\phi$ -value analysis usually measures the effects of conservative hydrophobic volume reduction mutants<sup>47</sup> but as the E and G5<sup>2</sup> subdomains lack a hydrophobic core and conservative substitution of solvent exposed residues rarely sufficiently destabilises proteins for reliable estimation of  $\phi$ -values, more radical substitutions have been included in this study. This approach has successfully been used to elucidate the "innate" ensemble-derived folding transition state for SasG. This previous study by the Clarke group showed that no intermediate  $\phi$ -values were obtained using similar substitutions to the ones used here, suggesting no major perturbation of the native or unfolded

states.<sup>32</sup> Additionally, large effects on the folded state of E-G5<sup>2</sup> of each substitution was obviated by CD and fluorescence emission spectra that were similar to pWT (E-G5<sup>2</sup>)<sub>5</sub> (Figure S6-S11).

The calculated  $\phi$ -values for all variants with a similar speed dependence of unfolding force to pWT (E-G5<sup>2</sup>)<sub>5</sub> are listed in Table 1 and shown schematically in Figure 4(B). For each variant,  $\phi$ -values for the subdomain in the E-G5<sup>2</sup> repeat without the substitution of ~1 demonstrates the quality of these data and the robustness of our approach. Mechanical  $\phi$ -value analysis is inherently low throughput due to both the need to produce polyproteins and obtain statistically robust force unfolding data at a range of retraction velocities. Examination of ensemble-derived  $\phi$ -values shows that these change gradually throughout the transition-state structure,<sup>44</sup> suggesting that our sampling (which is the highest reported to date for mechanical analyses) is sufficient to elucidate the coarse TS structure as substitutions have

been introduced throughout the structures of both subdomains. The data in Table 1 and shown schematically in Figure 4, reveal a largely native-like TS.

Figure 4(B) suggests that both the E-G5<sup>2</sup> interface (G517A and P549A) and the collagen-like regions of both E (G524A and G527A) and G5<sup>2</sup> (G584A and G587A) subdomains have undergone structural remodeling at the mechanical TS, yielding  $\phi$ -values of 0.0–0.8 (Table 1). P562A (G5<sup>2</sup> subdomain) has a  $\phi$ -value of  $-0.1$ , suggesting that stabilising non-native contacts are formed at the mechanical TS.<sup>49</sup> This unusual value may, however, arise due to error associated with small  $\Delta\Delta G_{UN}$  values.<sup>44,48</sup> In contrast to these regions, several residues in the ‘mechanical clamp’ regions have  $\phi$ -values  $\sim 1$ , suggesting that they retain native-like contacts at the TS and that they are the main force-bearing regions for SasG.

## Discussion

Concatenating a single domain of SasG (E-G5<sup>2</sup>) and its variants into a pentameric homopolyprotein (pWT (E-G5<sup>2</sup>)<sub>5</sub>) has allowed the determinants of SasG mechanical strength to be elucidated. While an increase in the mechanical strength of the G5<sup>2</sup> subdomain of pWT (E-G5<sup>2</sup>)<sub>5</sub> relative to SasG could be ascribed to domain number and compliance effects,<sup>36</sup> the change in the malleability of the E subdomain was unexpected and is rationalised by the lack of G5-E interface in pWT (E-G5<sup>2</sup>)<sub>5</sub>. This hypothesis was confirmed by an E-G5<sup>2</sup> interfacial variant (N598A), which not only displayed a change in the malleability of the E subdomain, but also restored the  $x_U$  to that observed by native SasG.

Our  $\phi$ -value analysis (Figure 4(B)) confirms that the ‘mechanical clamp’ region is native at the TS, consistent with the MD predictions by Gruszka and colleagues.<sup>10</sup> Disrupting the long stretches of hydrogen bonding and sidechain packing interactions in this region resulted in a change in the mechanical phenotype, by decreasing the unfolding force or altering the TS position (or both). The ‘mechanical clamp’ motif is typically observed in proteins requiring mechanical strength to perform their function such as I27<sup>39</sup> and C7a.<sup>24</sup> The origin of this resistance to extension is thought to be due to the requirement to simultaneously break all of the non-covalent interactions between the pulling positions. As the majority of proteins are extended via their termini, such shearing generally occurs between directly hydrogen bonded parallel  $\beta$ -strands. As proteins with these structures have complex topology, it has been observed that increasing mechanical strength correlates with increasing relative contact order (RCO).<sup>19,50</sup> As shown in Supplementary Figure S24, while this correlation generally holds for both subdomains of

SasG, the higher mechanical strength of the G5<sup>2</sup> subdomain relative to E ( $\sim 150$  pN difference at a retraction speed of  $600 \text{ nms}^{-1}$ ), despite an identical RCO suggests that sequence in addition to topology plays an important role.

The mechanical properties of SasG are further tailored by contacts in the pseudo-hydrophobic core, similar to that observed for the effects of hydrophobic core substitutions in both Protein L<sup>29</sup> and Protein GB1.<sup>30</sup>

Comparing  $\Delta\Delta G_{UN}$  and  $\Delta F_U$  (Figure 4(A)) shows clearly that force resistance does not always correlate with  $\Delta G_{UN}$  (exemplified by G527A:  $\Delta F_{U,E} = \sim 40$  pN,  $\Delta\Delta G_{UN} = 4.9 \pm 0.8 \text{ kJ mol}^{-1}$  and V556P:  $\Delta F_{U,G5} = \sim 0$  pN,  $\Delta\Delta G_{UN} = 14.1 \pm 0.8 \text{ kJ mol}^{-1}$ ). The lack of correlation between changes in these parameters (Figure S25) is unsurprising<sup>29–30,44</sup> as  $\Delta G_{UN}$  measures the global equilibrium stability and  $F_U$  measures the kinetic stability of a localised structure between two defined extension points. This comparison identifies the collagen-like motif as an important factor in the mechanical strength of SasG as it has a large effect on force, despite a generally moderate effect on  $\Delta G_{UN}$ . As the  $\phi$ -value analysis suggests gross rearrangement of the collagen-like motif at the TS, we utilised MD to investigate this in more detail (Methods). These analyses displayed the elongation and untwisting of the collagen-like regions prior to global unfolding (Methods, Figure S26, Movie S1), which may bestow subtle flexibility of the collagen-like motif. The collagen-like regions may act as an intrinsic molecular spring when there are several in tandem, permitting dissipation of force and regulating the ability of the bacterial cell to sustain attachment under shear force by preventing the global unfolding of the E and G5<sup>2</sup> subdomains, in accord with the low (0) and partial  $\phi$ -values observed for residues 524 and 527 (in E) and 584 and 587 (in G5<sup>2</sup>).

G524/G527 (E subdomain) and G584/G587 (G5<sup>2</sup> subdomain) pairs are structurally equivalent glycine residues located in one of the three left-handed polyproline PPII-like helices following the canonical collagen sequence of X<sub>aa</sub>Y<sub>aa</sub>Gly with glycine required to accommodate the packing of the sidechains at the central axis.<sup>51</sup> Here we have shown that substitution of these glycines with residues with bulkier side-chains results in a large decrease in  $F_U$  for SasG. This is probably due to the structural perturbation that arises from overpacking (Figure S27). This type of substitution is also found in OI – a rare genetic disease (brittle bone disease) affecting the connective tissues characterised by extremely fragile bones that break or fracture easily. Structural and MD studies on collagen-like peptides show that accommodation of a methyl side-chain results in local twist relaxation and bulging due to loss of hydrogen bonding and electrostatic repulsions (Figure S27).<sup>52–53</sup> In line with this observation, spectroscopic analysis of our variants displays a subtle deviation in sec-

ondary structure (Figure S8) indicating similar structural perturbation of our collagen-like regions. In summary, OI-like substitutions significantly decrease the mechanical strength of the E and G5<sup>2</sup> subdomains, identifying the collagen-like region as a novel mechanical motif. We speculate that the changes in mechanical phenotype uncovered for SasG, also affects the mechanical properties of collagen fibres found in OI patients.

## Materials and Methods

### Homo-polyprotein construction by Golden Gate assembly

Polymerase chain reactions (PCR) were performed with Q5<sup>®</sup> DNA polymerase (NEB, Hertfordshire, UK). All mutagenic, cassette amplification and destination vector linearisation primers are found in Tables S42-S46. Briefly, a gene encoding a monomer of E-G5<sup>2</sup> (using a *E. coli* optimised native SasG sequence as template, provided by Professor Jennifer Potts, University of Sydney, Australia) was inserted into a linearised pET14b vector using Gibson Assembly<sup>®</sup>.<sup>54</sup> This WT E-G5<sup>2</sup> monomer sequence was then used as template to make pentameric polyproteins of the wild-type and variant sequences by Golden Gate assembly. Firstly, two Bsal restriction sites were removed from the destination pET14b vector by PCR to create pET14bΔ*bsal*. For each construct, five DNA cassettes were generated by PCR that encoded one E-G5<sup>2</sup> repeat and part of the unstructured linkers separating each repeat together with Bsal sites (at the DNA level) for assembly. The purified cassettes and PCR-linearised pET14bΔ*bsal* were then assembled using the NEB Golden Gate assembly kit (Bsal-HF<sup>®</sup>v2) following the manufacturers protocol, using 75 ng of linearised destination vector and a twofold molar excess of cassettes. The reaction mixture was thermo-cycled (T100<sup>™</sup> thermal cycler, BioRad, California, USA) at 37 °C for 1 min and then 16 °C for 1 min for a total of 30 cycles. Subsequently, the mixture was then held at 60 °C for 5 min. 2 μL of the product was transformed into SURE2 competent *E. coli* cells (Agilent, California, USA). The sequence of each assembled variant was confirmed by Sanger Sequencing (Twist Bioscience, Cambridge, UK). The final construct (and variants thereof) comprises five identical domains of E-G5<sup>2</sup> separated by unstructured linkers and two C-terminal cysteine residues for protein immobilisation to gold substrate for SMFS experiments:

MSSHHHHHSS(E-G5<sup>2</sup>)LSVGATI(E-G5<sup>2</sup>)TVIGLAS  
(E-G5<sup>2</sup>)ALSGTIV(E-G5<sup>2</sup>)VITGSLA(E-G5<sup>2</sup>)CC

The full protein sequence of pWT (E-G5<sup>2</sup>)<sub>5</sub> and variants thereof are found in [Supplementary Information](#).

### Protein over-expression and purification

Plasmids encoding the homo-polyprotein constructs were transformed into *E. coli* BL21 (DE3) pLysS (Agilent, California, USA). 10 × 0.5 L of autoinduction medium (1% (w/v) yeast extract, 2% (w/v) bactotryptone, 0.01% (w/v) glycerol, 0.001% (w/v) D-glucose anhydrous, 0.004% (w/v) α-Lactose monohydrate, 50 mM ammonium chloride, 5 mM sodium sulphate, 25 mM potassium phosphate monobasic, 25 mM sodium phosphate dibasic, 100 μg/mL ampicillin and 25 μg/mL chloramphenicol) was inoculated with overnight starter culture (LB medium containing 100 μg/mL ampicillin and 25 μg/mL chloramphenicol) and protein expression carried out at 28 °C, 200 rpm as described.<sup>55</sup> After 24 h, the cells were harvested and the cell pellet resuspended in lysis buffer (20 mM Na<sub>2</sub>HPO<sub>4</sub>-NaH<sub>2</sub>PO<sub>4</sub>, 8 M urea, 500 mM NaCl, 10 mM imidazole, 2 mM DTT, 1 mM PMSF, 2 mM benzamidine and a rice grain of lysozyme and DNaseI). After cell disruption by sonication the cleared lysate was applied to a lab-packed 200 mL pre-charged Ni Sepharose<sup>™</sup> Fast Flow column (Cytiva, Massachusetts, USA). Wash/refolding buffer (20 mM Na<sub>2</sub>HPO<sub>4</sub>-NaH<sub>2</sub>PO<sub>4</sub>, 500 mM NaCl, 10 mM imidazole, 2 mM DTT, 1 mM PMSF, 2 mM benzamidine) was applied until baseline A<sub>280</sub> was achieved and the protein eluted using wash buffer supplemented with 150 mM imidazole. The protein of interest was dialysed into 20 mM Tris-HCl, 50 mM NaCl, 1 mM EDTA and 2 mM DTT for 16 h. This was loaded onto 2 × 5 mL HiTrap SP HP columns (Cytiva) stacked atop of 4 × 5 mL HiTrap Q HP columns (Cytiva). After removal of the HiTrap SP HP columns, the protein was eluted with a linear 50–185 mM NaCl gradient of 7.5 column volumes. Subsequent purification was performed with gel filtration using a 320 mL Hiload Superdex<sup>™</sup> 26/600 75 column (Cytiva) in 1 × PBS, pH 7.4. Successful isolation was confirmed by LC-MS (Table S6). The recombinant protein was snap frozen in liquid nitrogen and stored at –80 °C.

### Circular dichroism spectroscopy

200 μL of 0.2 mg/mL protein solution (5 mM NaH<sub>2</sub>PO<sub>4</sub>, pH 7.4) was transferred to a 1 mm path-length cuvette (Hellma, Müllheim, Germany). A far-UV spectrum (180–260 nm) was obtained using a 2 nm bandwidth, 1 s time step (25 °C) with an average of three scans per sample on a Chirascan CD spectrometer (Applied Photophysics<sup>®</sup>, Leatherhead, UK).

### Single-molecule force spectroscopy

Single-molecule force spectroscopy experiments were carried out for the native SasG construct (G5<sup>1</sup>-G5<sup>7</sup>), pWT (E-G5<sup>2</sup>)<sub>5</sub> and variants as described previously.<sup>10</sup> Briefly, an MFP-3D<sup>™</sup> Stand

Alone AFM (Asylum Research, Buckinghamshire, UK) was mounted with a silicon nitride cantilever (MLCT, Bruker, California, USA). The deflection sensitivity and natural resonance of the cantilever were found, and the spring constant calculated using the equi-partition theorem.<sup>56</sup> 100  $\mu\text{L}$  250  $\mu\text{g}/\text{mL}$  of protein in PBS, pH 7.4 was deposited on a freshly cleaved gold substrate,<sup>10</sup> resulting in covalent attachment between the C-terminal cysteine residues and the gold atoms of the surface. After incubation for  $\sim 15$  min, the surface was washed with PBS, pH 7.4 and allowed to equilibrate for another 15 min prior to accumulating force-extension data. Mechanical unfolding experiments were carried out at retraction velocities of 200, 800, 1500, 3000 and 5000  $\text{nms}^{-1}$  at room temperature over a distance of 600 nm, with the exception of V522P (E-G5<sup>2</sup>)<sub>5</sub> and V550P (E-G5<sup>2</sup>)<sub>5</sub>, which were carried out at 200 and 5000  $\text{nms}^{-1}$ . Three separate cantilevers were used for each construct, with the exception of V522P (E-G5<sup>2</sup>)<sub>5</sub> and V550P (E-G5<sup>2</sup>)<sub>5</sub> ( $n = 1$ ), to decrease systematic errors from cantilever spring constant calculation.

### Analysis of single-molecule force spectroscopy data

Data were filtered to include only traces that display the unfolding of four or more subdomains and a detachment peak. All mechanical unfolding data were processed using IGOR pro (version 6.37, Wavemetrics, Oregon, USA) with an Asylum Research extension (MFP3DXop v30). After filtering, spectra were imported into Fodis.<sup>57</sup> The apex of each peak was taken as the observed unfolding force and  $L_C$  values obtained by fitting a worm-like chain (WLC) model for polymer elasticity<sup>35</sup>:

$$F(x) = \frac{k_B T}{p} \left( 0.25(1 - \frac{x}{L_C})^{-2} - 0.25 + \frac{x}{L_C} \right)$$

Where  $L_C$  is the contour length (maximum predicted extension of the polypeptide chain under external force),  $F(x)$  is the force as a function of extension,  $x$ .  $k_B$  is the Boltzmann's constant,  $T$  is temperature and a persistence length ( $p$ ) of 3.8  $\text{\AA}$ . Both the unfolding forces and  $\Delta L_C$  were binned and plotted in histograms, with bin sizes of 10 pN and 5  $\text{\AA}$ , respectively. Gaussian fits to these histograms were used to obtain the mode from each cantilever repeat, which were averaged to yield the mean unfolding force and  $\Delta L_C$  value.

### Equilibrium denaturation

Fluorescence spectroscopy was performed on a Photon Technology International spectrofluorometer (PTI, New Jersey, USA) at 25  $^{\circ}\text{C}$  using a 1 mL quartz Hellma cuvette (Hellma, Müllheim, Germany). For equilibrium denaturation of pWT (E-G5<sup>2</sup>)<sub>5</sub> and variants thereof, PBS pH 7.4 and PBS, 9 M urea pH 7.4 were prepared alongside

1 mg/mL of the protein being analysed in PBS pH 7.4. Five stocks of 0.2 mg/mL protein containing 0, 2, 4, 6 and 8 M urea were prepared and mixed to create protein samples increasing in urea concentration in 0.2 M increments from 0 to 8 M. After equilibration for 16 h at 25  $^{\circ}\text{C}$  in a circulating water bath (NesLab, Massachusetts, USA), the samples were transferred to the fluorimeter and after 5 min of equilibration, the sample was excited at 276 nm and a time drive scan was taken at 305 nm for 30 seconds (1 second per data point) at 25  $^{\circ}\text{C}$ . The average signal was calculated for each concentration and plot as a function of urea concentration. A standard two-state transition chemical denaturant model<sup>58</sup> was fit to the data using Igor Pro (version 7.02, Wavemetrics, Oregon, USA) to obtain thermodynamic fitting values. For all variants (with the exception of pWT (E-G5<sup>2</sup>), I502P, V522P, and V550P), the  $m_{UN}$  value was fixed to 6  $\text{kJ mol}^{-1} \text{M}^{-1}$  (the value extracted for pWT (E-G5<sup>2</sup>)<sub>5</sub>). The raw data was normalised to a fraction of natively folded protein to allow qualitative comparison between pWT (E-G5<sup>2</sup>)<sub>5</sub> and variants thereof.

### Mechanical $\phi$ -value analysis

$\Delta\Delta G_{UN}$  values are the difference of the thermodynamic stability ( $\Delta G_{UN}$ ) between each variant and pWT (E-G5<sup>2</sup>)<sub>5</sub>. The  $\Delta\Delta G_{TS-N}^{WT-MUT}$  values of variants were calculated directly from the speed dependence as described previously<sup>40</sup>:

$$\Delta\Delta G_{TS-N}^{WT-MUT} = RT(f_{WT} - f_{MUT})/m$$

Where  $f_{WT}$  and  $f_{MUT}$  are the average unfolding forces of pWT (E-G5<sup>2</sup>)<sub>5</sub> and the variant being measured, respectively.  $R$  is the gas constant,  $T$  is temperature and  $m$  is the average gradient of the weighted best-fits to the speed dependence of unfolding force for those variants and subdomains within error (of the gradient value) of pWT (E-G5<sup>2</sup>)<sub>5</sub> at a retraction velocity of 1500  $\text{nms}^{-1}$ . Errors were propagated using an error of 5% (lower confidence limit due to inherent cantilever calibration systematic error) and errors on  $\Delta\Delta G_{UN}$  were the propagated errors of the fits.  $\phi$ -value can then be calculated:

$$\phi = 1 - \frac{\Delta\Delta G_{TS-N}^{WT-MUT}}{\Delta\Delta G_{UN}}$$

### E-G5<sup>2</sup> forced unfolding simulations

Simulations were carried out using an all atom force field (CHARMM22) and fast analytical continuum treatment of solvation (FACTS) implicit solvent model. Forced unfolding was simulated by attaching an ideal spring to the N and C atoms of the two termini and retracting them at a constant velocity (in the range  $10^5$ - $10^7$   $\text{nms}^{-1}$ ) at 300 K and 0 K (local minimum energy pathway). The main

features of the unfolding pathways does not depend on the pulling speed or the temperature.

### CRedit authorship contribution statement

**Alexander J.E. Bruce:** Investigation, Conceptualization, Methodology, Validation, Writing – original draft. **Emanuele Paci:** Software, Resources, Data curation, Supervision, Writing – review & editing. **David J. Brockwell:** Conceptualization, Methodology, Resources, Project administration, Supervision, Writing – review & editing.

### DECLARATION OF COMPETING INTERESTS

The authors declare that they have no known competing financial interests or personal relationships that could have appeared to influence the work reported in this paper.

### Acknowledgments

The authors would like to thank Professor Jennifer Potts for a gift of the *E. coli* codon-optimised native SasG DNA and Professor Sheena Radford and members of the Radford, Brockwell, and Calabrese groups for helpful discussions and advice throughout. This work was supported by a White Rose Research Studentship (White Rose University Consortium) to A.J.E.B. We thank the Wellcome Trust (094232) and University of Leeds for the purchase of the Chiroscan CD spectrometer.

### Appendix A. Supplementary Data

Supplementary data to this article can be found online at <https://doi.org/10.1016/j.jmb.2023.167980>.

Received 18 October 2022;

Accepted 19 January 2023;

Available online 25 January 2023

#### Keywords:

Single-molecule force spectroscopy (SMFS);  
protein unfolding;  
SasG;  
mechanobiology;  
collagen-related disease and osteogenesis imperfecta (OI)

† Present address: University of Bologna, Department of Physics, Bologna, Italy.

#### Abbreviations:

Aap, accumulation-associated protein; AFM, Atomic Force Microscopy; CLM, collagen-like motif; CWA, cell-wall anchored; *E. coli*, *Escherichia coli*;  $F_U$ , unfolding force; FWHM, full width at half maximum; LC-MS, liquid

chromatography-mass spectroscopy; MD, molecular dynamic; OI, Osteogenesis Imperfecta; PBS, phosphate buffered saline; PPII, Polyproline II; SasG, *S. aureus* surface protein G; *S. aureus*, *Staphylococcus aureus*; SMFS, single-molecule force spectroscopy; TS, transition state; WLC, worm-like chain; WT, wild-type

### References

- Costerton, J.W., Lewandowski, Z., Caldwell, D.E., Korber, D.R., Lappin-Scott, H.M., (1995). Microbial Biofilms. *Annu. Rev. Microbiol.* **49**, 711–745.
- Otto, M., (2014). Physical stress and bacterial colonisation. *FEMS Microbiol. Rev.* **38**, 1250–1270.
- Herman, P., El-Kirat-Chatel, S., Beaussart, A., Geoghegan, J.A., Foster, T.J., Dufrêne, Y.F., (2014). The binding force of the staphylococcal adhesion SdrG is remarkably strong. *Mol. Microbiol.* **93**, 356–368.
- Herman-Bausier, P., Labate, C., Towell, A.M., Derclaye, S., Geoghegan, J.A., Dufrêne, Y.F., (2018). *Staphylococcus aureus* clumping factor A is a force-sensitive molecular switch that activates bacterial adhesion. *PNAS* **115**, 5564–5569.
- Mathelié-Guinlet, M., Viela, F., Pietrocola, G., Speziale, P., Alsteens, D., Dufrêne, Y.F., (2020). Force-clamp spectroscopy identifies a catch bond mechanism in a Gram-positive pathogen. *Nature Commun.* **11**, 5431.
- Grandbois, M., Beyer, M., Rief, M., Clausen-Schaumann, H., Gaub, H.E., (1999). How strong is a covalent bond. *Science* **283**, 1727–1730.
- Miller, E., Garcia, T., Hultgren, S., Oberhauser, A.F., (2006). The mechanical properties of *E. coli* type 1 pili measured by Atomic Force Microscopy techniques. *Biophys. J.* **91**, 3848–3856.
- Whelan, F., Lafita, A., Gilbert, J., Dégut, C., Griffiths, S.C., Jenkins, H.T., St John, A.N., Paci, E., et al., (2021). Periscope Proteins are variable-length regulators of bacterial cell surface interactions. *PNAS* **118**, e2101349118
- Chantraine, C., Mathelié-Guinlet, M., Pietrocola, G., Speziale, P., Dufrêne, Y.F., (2021). AFM identifies a protein complex involved in pathogen adhesion which ruptures at three nanonewtons. *Nano Lett.* **21**, 7595–7601.
- Gruszka, D.T., Whelan, F., Farrance, O.E., Fung, H.K.H., Paci, E., Jeffries, C.M., Svergun, D.I., Baldock, C., et al., (2015). Cooperative folding of intrinsically disordered domains drives assembly of a strong elongated protein. *Nature Commun.* **6**, 7271.
- Corrigan, R.M., Rigby, D., Handley, P., Foster, T.J., (2007). The role of *Staphylococcus aureus* surface protein SasG in adherence and biofilm formation. *Microbiology (Reading)* **153**, 2435–2446.
- Roche, F.M., Meehan, M., Foster, T.J., (2003). The *Staphylococcus aureus* surface protein SasG and its homologues promote bacterial adherence to human desquamated nasal epithelial cells. *Microbiology (Reading)* **149**, 2759–2767.
- Formosa-Dague, C., Speziale, P., Foster, T.J., Geoghegan, J.A., Dufrêne, Y.F., (2016). Zinc-dependent mechanical properties of *Staphylococcus aureus* biofilm-forming surface protein SasG. *PNAS* **113**, 410–415.
- Conrady, D.G., Brescia, C.C., Horii, K., Weiss, A.A., Hassett, D.J., Herr, A.B., (2008). A zinc-dependent

- adhesion module is responsible for intercellular adhesion in staphylococcal biofilms. *PNAS* **105**, 19456–19461.
15. Roche, F.M., Massey, R., Peacock, S.J., Day, N.P.J., Visai, L., Speziale, P., Lam, A., Pallen, M., et al., (2003). Characterization of novel LPXTG-containing proteins of *Staphylococcus aureus* identified from genome sequences. *Microbiology (Reading)* **149**, 643–654.
  16. Gruszka, D.T., Wojdyla, J.A., Bingham, R.J., Turkenburg, J.P., Manfield, I.W., Steward, A., Leech, A.P., Geoghegan, J.A., et al., (2012). Staphylococcal biofilm-forming protein has a contiguous rod-like structure. *PNAS* **109**, E1011–E1018.
  17. Kramer, R.Z., Bella, J., Mayville, P., Brodsky, B., Berman, H.M., (1999). Sequence dependent conformational variations of collagen triple-helical structure. *Nature Struct. Biol.* **6**, 454–457.
  18. Bozec, L., Horton, M., (2005). Topography and mechanical properties of single molecules of type I collagen using Atomic Force Microscopy. *Biophys. J.* **88**, 4223–4231.
  19. Hoffmann, T., Tych, K.M., Hughes, M.L., Brockwell, D.J., Dougan, L., (2013). Towards design principles for determining the mechanical stability of proteins. *PCCP* **15**, 15767–15780.
  20. Crampton, N., Brockwell, D.J., (2010). Unravelling the design principles for single protein mechanical strength. *Curr. Opin. Struct. Biol.* **20**, 508–517.
  21. Hughes, M.L., Dougan, L., (2016). The physics of pulling polypeptides: A review of single molecule force spectroscopy using the AFM to study protein unfolding. *Rep. Prog. Phys.* **79**, 076601
  22. Sikora, M., Sułkowska, J.I., Witkowski, B.S., Cieplak, M., (2011). BSDB: the biomolecule stretching database. *Nucleic Acids Res.* **39**, D443–D450.
  23. Sikora, M., Sułkowska, J.I., Cieplak, M., (2009). Mechanical strength of 17,134 model proteins and cysteine slipknots. *PLoS Comput. Biol.* **5**, e1000547.
  24. Valbuena, A., Oroz, J., Hervás, R., Vera, A.M., Rodríguez, D., Menéndez, M., Sulkowska, J.I., Cieplak, M., et al., (2009). On the remarkable mechanostability of scaffolds and the mechanical clamp motif. *PNAS* **106**, 13791–13796.
  25. Milles, L.F., Unterauer, E.M., Nicolaus, T., Gaub, H.E., (2018). Calcium stabilizes the strongest protein fold. *Nature Commun.* **9**, 4764.
  26. Oude Vrielink, A.S., Vance, T.D.R., de Jong, A.M., Davies, P.L., Voets, I.K., (2017). Unusually high mechanical stability of bacterial adhesin extender domains having calcium clamps. *PLoS One* **12**, e0174682.
  27. Wang, B., Xiao, S., Edwards, S.A., Gräter, F., (2013). Isopeptide bonds mechanically stabilize spy0128 in bacterial pili. *Biophys. J.* **104**, 2051–2057.
  28. Herman-Bausier, P., Valotteau, C., Pietrocola, G., Rindi, S., Alsteens, D., Foster, T.J., Speziale, P., Dufrêne, Y.F., (2016). Mechanical strength and inhibition of the *Staphylococcus aureus* collagen-binding protein Cna. *MBio* **7**, e01529.
  29. Sadler, D.P., Petrik, E., Taniguchi, Y., Pullen, J.R., Kawakami, M., Radford, S.E., Brockwell, D.J., (2009). Identification of a mechanical rheostat in the hydrophobic core of protein L. *J. Mol. Biol.* **393**, 237–248.
  30. Bu, T., Wang, H.C.E., Li, H., (2012). Single molecule force spectroscopy reveals critical roles of hydrophobic core packing in determining the mechanical stability of protein GB1. *Langmuir* **28**, 12319–12325.
  31. Carrión-Vázquez, M., Oberhauser, A.F., Fisher, T.E., Marszalek, P.E., Li, H., Fernandez, J.M., (2000). Mechanical design of proteins studied by single-molecule force spectroscopy and protein engineering. *Prog. Biophys. Mol. Biol.* **74**, 63–91.
  32. Gruszka, D.T., Mendonça, C.A.T.F., Paci, E., Whelan, F., Hawkhead, J., Potts, J.R., Clarke, J., (2016). Disorder drives cooperative folding in a multidomain protein. *PNAS* **113**, 11841–11846.
  33. Hoffmann, T., Tych, K.M., Crosskey, T., Schiffrin, B., Brockwell, D.J., Dougan, L., (2015). Rapid and robust polypeptide production facilitates single-molecule mechanical characterization of  $\beta$ -Barrel Assembly Machinery Polypeptide Transport Associated domains. *ACS Nano* **9**, 8811–8821.
  34. Bustamante, C., Marko, J.F., Siggia, E.D., Smith, S., (1994). Entropic elasticity of  $\lambda$ -phage DNA. *Science* **265**, 1599–1600.
  35. Marko, J.F., Siggia, E.D., (1995). Stretching DNA. *Macromolecules* **28**, 8759–8770.
  36. Zinober, R.C., Brockwell, D.J., Beddard, G.S., Blake, A.W., Olmsted, P.D., Radford, S.E., Smith, D.A., (2002). Mechanically unfolding proteins: The effect of unfolding history and the supramolecular scaffold. *Protein Sci.* **11**, 2759–2765.
  37. Brockwell, D.J., Beddard, G.S., Clarkson, J., Zinober, R.C., Blake, A.W., Trinick, J., Olmsted, P.D., Smith, D.A., et al., (2002). The effect of core destabilization on the mechanical resistance of I27. *Biophys. J.* **83**, 458–472.
  38. Myers, J.K., Pace, C.N., Scholtz, J.M., (1995). Denaturant m values and heat capacity changes: relation to changes in accessible surface areas of protein unfolding. *Protein Sci.* **4**, 2138–2148.
  39. Li, H., Carrión-Vázquez, M., Oberhauser, A.F., Marszalek, P.E., Fernandez, J.M., (2000). Point mutations alter the mechanical stability of immunoglobulin modules. *Nature Struct. Biol.* **7**, 1117–1120.
  40. Best, R.B., Fowler, S.B., Toca-Herrera, J.L., Clarke, J., (2002). A simple method for probing the mechanical unfolding pathway of proteins in detail. *PNAS* **99**, 12143–12148.
  41. Evans, E., (2001). Probing the relation between force–lifetime–and chemistry in single molecular bonds. *Annu. Rev. Biophys. Biomol. Struct.* **30**, 105–128.
  42. Anderson, K.L., Radford, S.E., Smith, D.A., Brockwell, D. J., (2008). The dynamical response of proteins under force. *In: Handbook of Molecular Force Spectroscopy*. Springer, New York, pp. 202–246.
  43. Schlierf, M., Rief, M., (2005). Temperature softening of a protein in single-molecule experiments. *J. Mol. Biol.* **354**, 497–503.
  44. Best, R.B., Fowler, S.B., Herrera, J.L.T., Steward, A., Paci, E., Clarke, J., (2003). Mechanical unfolding of a titin Ig domain: structure of transition state revealed by combining atomic force microscopy, protein engineering and molecular dynamics simulations. *J. Mol. Biol.* **330**, 867–877.
  45. Ng, S.P., Rounsevell, R.W.S., Steward, A., Geierhaas, C. D., Williams, P.M., Paci, E., Clarke, J., (2005). Mechanical unfolding of TNfn3: The unfolding pathway of a FnIII domain probed by protein engineering, AFM and MD simulation. *J. Mol. Biol.* **350**, 776–789.

46. Rounsevell, R., Forman, J.R., Clarke, J., (2004). Atomic force microscopy: Mechanical unfolding of proteins. *Methods* **34**, 100–111.
47. Fersht, A.R., Matouschek, A., Serrano, L., (1992). The folding of an enzyme: I. Theory of protein engineering analysis of stability and pathway of protein folding. *J. Mol. Biol.* **224**, 771–782.
48. Sánchez, I.E., Kiefhaber, T., (2003). Origin of unusual  $\phi$ -values in protein folding: evidence against specific nucleation sites. *J. Mol. Biol.* **334**, 1077–1085.
49. Zarrine-Afsar, A., Wallin, S., Neculai, A.M., Neudecker, P., Howell, P.L., Davidson, A.R., Chan, H.S., (2008). Theoretical and experimental demonstration of the importance of specific nonnative interactions in protein folding. *PNAS* **105**, 9999–10004.
50. Huysmans, G.H.M., Baldwin, S.A., Brockwell, D.J., Radford, S.E., (2010). The transition state for folding of an outer membrane protein. *PNAS* **107**, 4099–4104.
51. Shoulders, M.D., Raines, R.T., (2009). Collagen structure and stability. *Annu. Rev. Biochem.* **78**, 929–958.
52. Bella, J., Eaton, M., Brodsky, B., Berman, H.M., (1994). Crystal and molecular structure, of a collagen-like peptide at 1.9 Å resolution. *Science* **266**, 75–81.
53. Punitha, V., Raman, S.S., Parthasarathi, R., Subramanian, V., Rao, J.R., Nair, B.U., Ramasami, T., (2009). Molecular dynamics investigations on the effect of D amino acid substitution in a triple-helix structure and the stability of collagen. *J. Phys. Chem. B* **113**, 8983–8992.
54. Gibson, D.G., Young, L., Chuang, R.-Y., Venter, J.C., Hutchison, C.A., Smith, H.O., (2009). Enzymatic assembly of DNA molecules up to several hundred kilobases. *Nature Methods* **6**, 343–345.
55. Studier, F.W., (2005). Protein production by auto-induction in high density shaking cultures. *Protein Expr. Purif.* **41**, 207–234.
56. Hutter, J.L., Bechhoefer, J., (1993). Calibration of atomic-force microscope tips. *Rev. Sci. Instrum.* **64**, 1868.
57. Galvanetto, N., Perissinotto, A., Pedroni, A., Torre, V., (2018). Fodis: software for protein unfolding analysis. *Biophys. J.* **114**, 1264–1266.
58. Santoro, M.M., Bolen, D.W., (1988). Unfolding free energy changes determined by the linear extrapolation method. 1. Unfolding of phenylmethanesulfonyl  $\alpha$ -chymotrypsin using different denaturants. *Biochemistry* **27**, 8063–8068.